Journal of Catalysis 256 (2008) 293–300

Contents lists available at ScienceDirect

Journal of Catalysis

www.elsevier.com/locate/jcat

Dehydrogenation of propane over spinel-type gallia–alumina solid solution catalysts

Miao Chen, Jie Xu, Fang-Zheng Su, Yong-Mei Liu, Yong Cao *, He-Yong He, Kang-Nian Fan

Department of Chemistry and Shanghai Key Laboratory of Molecular Catalysis and Innovative Materials, Fudan University, Shanghai 200433, PR China

ARTICLE INFO

Article history:
Received 24 February 2008
Revised 24 March 2008
Accepted 25 March 2008
Available online 23 April 2008

Keywords:
Propane
Dehydrogenation
Gallia–alumina
Spinel
Solid solution
Lewis acidity

ABSTRACT

Dehydrogenation of propane to propylene in the presence or absence of carbon dioxide was performed over a series of mixed $Ga_xAl_{10-x}O_{15}$ oxides (with x varying from 0 to 10) synthesized through an alcoholic coprecipitation pathway. Among the various compositions of $Ga_xAl_{10-x}O_{15}$, the maximum activity was observed for $x = 8$. Whereas the same tendency was observed for the specific activity normalized by BET surface area, significantly enhanced stability was achieved for Ga_2O_3–Al_2O_3 with higher aluminum content. A correlation between the NH_3-TPD results and the initial activity for $Ga_xAl_{10-x}O_{15}$ reveals that a high population of surface acid sites related to tetrahedral Ga^{3+} cations is important to achieving high activity. The specific interaction between Ga_2O_3 and Al_2O_3 due to the formation of spinel-type γ-Ga_2O_3–Al_2O_3 solid solutions is suggested to play a key role in the dispersion and distribution of surface gallium sites, which makes $Ga_xAl_{10-x}O_{15}$ composites highly active and stable for the reaction.

1. Introduction

The catalytic dehydrogenation of alkanes is a process of considerable importance, because it represents a route for obtaining alkenes from poorly reactive and low-cost saturated feedstocks [1–3]. In this respect, an important reaction is the dehydrogenation of propane to propylene [4–6]. This process is of increasing significance due to the limited capabilities of steam cracking and fluid catalytic cracking to meet the increasing demands of the propylene market [7–9]. In this sense, chromium oxide-based catalysts have been used for the dehydrogenation of propane in the absence of hydrogen as a co-feed gas [10–12], and platinum-based catalysts have been used for the dehydrogenation of propane in the presence of hydrogen [13–16]. From environmental and practical standpoints, however, chromium-free catalysts are highly desirable for the dehydrogenation of propane in the absence of hydrogen [5].

In recent years, Ga_2O_3-based catalysts have attracted interest as potential candidates for alkane dehydrogenation processes [5, 17–21]. This was prompted by Nakagawa's reports of exceptionally high activity of the commercial Ga_2O_3 for the dehydrogenation of ethane to ethylene in the presence of CO_2 [20]. Although commercial Ga_2O_3 has been shown to be far superior for the ethane dehydrogenation reaction compared with Cr_2O_3 and V_2O_5 catalysts, some recent studies have demonstrated that supported gallium oxides can be more active and stable for the dehydrogenation of light alkanes [5,21–23]. In particular, promising results have been obtained when the Ga_2O_3 catalysts are dispersed on an inert oxide support, such as TiO_2 or Al_2O_3 [21,23], which were found to be quite active in the propane dehydrogenation reaction even at temperatures as low as 773 K [23]. Other Ga_2O_3-based systems evaluated in the recent literature as alkane dehydrogenation catalysts include different polymorphs of Ga_2O_3, such as α-, β-, γ-, and δ-Ga_2O_3 [24].

Despite extensive efforts dedicated to the reaction mechanism and the factors that control activity, the aforementioned Ga_2O_3-based catalysts all deactivate drastically within a few hours [21, 23,24], because a high density of medium-strong acid sites on the surface of the Ga_2O_3-based materials favors considerable coke formation under alkane dehydrogenation conditions [21,23,25]. Neutralizing the acid sites by introducing potassium to the gallium oxide system has been used in propane dehydrogenation in an effort to suppress coke deposition [4]; however, this leads only to a drastic drop in catalytic activity. In the continuing search for more effective technologies for propylene production [4–6], there is a definite need for new, improved gallia-based catalysts that can allow efficient and stable dehydrogenation of propane in the presence of carbon dioxide under mild conditions.

Based on their superior ability to activate hydrocarbon species, gallia–alumina solid solutions have attracted considerable recent attention as excellent materials for the selective catalytic reduction (SCR) of NO_x by hydrocarbons owing to their unique surface acidity properties [26–30]. To the best of our knowledge, however, the use of Ga_2O_3–Al_2O_3 solid solutions as catalysts in the alkane dehydrogenation reaction has not yet been reported. In the present study, we investigated the development of a new, efficient Ga_2O_3–Al_2O_3 solid solution system exhibiting significantly enhanced activity and

* Corresponding author. Fax: +86 21 55665287.
E-mail address: yongcao@fudan.edu.cn (Y. Cao).

0021-9517/$ – see front matter
doi:10.1016/j.jcat.2008.03.021

stability for the catalytic dehydrogenation of propane. Our results demonstrate that the formation of gallia–alumina solid solution between Ga_2O_3 and Al_2O_3 can allow the favorable creation of a higher population of surface gallium sites with weak Lewis acidity, which makes the Ga_2O_3-based catalysts highly active and stable for the reaction.

2. Experimental

2.1. Catalyst preparation

A series of mixed Ga_2O_3–Al_2O_3 oxide catalysts with various compositions as well as the simple oxide of Al_2O_3 and Ga_2O_3 were prepared through an alcoholic coprecipitation pathway [31]. In a typical synthesis, concentrated aqueous ammonia (28 wt%) and ethanol (50:50 in volume) was added dropwise to the ethanol solution of gallium nitrate hydrate (Aldrich, 99.99%) and aluminum nitrate hydrate (Fluka, 99.9%) with different Ga:Al molar ratio until pH ca. 8.5 and no further precipitation occurred. The resulting gel was quickly filtered and thoroughly washed by ethanol, dried at 373 K overnight, and finally calcined at 773 K for 6 h.

2.2. Catalyst characterization

The BET specific surface areas of the samples were determined by adsorption–desorption of nitrogen at liquid nitrogen temperature using a Micromeritics TriStar 3000 instrument. Powder X-ray diffraction (XRD) of the catalysts was carried out on a Germany Bruker D8Advance X-ray diffractometer using nickel-filtered Cu$K\alpha$ radiation at 40 kV and 20 mA. The acidic property of each catalyst was characterized by NH_3-TPD. NH_3 was adsorbed at 393 K after pretreatment at 773 K in a He stream. The desorbed NH_3 in flowing He gas was quantified (NH_2 fragment of mass number 16) by mass spectroscopy (Balzers OmniStar) at 393–873 K (ramp rate, 10 K min^{-1}). To characterize the nature of the acid sites, spectra of chemisorbed pyridine were obtained with a Bruker Vector 22 spectrometer using self-supporting wafers in a heatable IR gas cell. The samples were pretreated at 773 K for 1 h under vacuum before pyridine adsorption. Pyridine was adsorbed at room temperature from an argon flow containing 2 vol% pyridine, after which the samples were heated to 373 K and evacuated to remove physisorbed and weakly chemisorbed pyridine. Each spectrum was obtained by subtracting the background (base spectrum) of the unloaded sample.

The XPS spectra of the samples were obtained with a Perkin–Elmer PHI 5000C spectrometer working in the constant analyzer energy mode with Mg$K\alpha$ radiation as the excitation source. The carbonaceous C 1s line (284.6 eV) was used as the reference to calibrate the binding energies (BEs). Elemental analysis was performed using ion-coupled plasma (ICP) atomic emission spectroscopy on a Thermo Electron IRIS Intrepid II XSP spectrometer. Thermogravimetric analysis (TGA) was conducted on a Perkin–Elmer TGA-7 analyzer to determine the amount of coke deposited on the catalyst after the reaction. Twenty milligrams of sample was heated from room temperature to 873 K at a heating rate of 10 K min^{-1} in flowing air. ^{71}Ga MAS NMR measurements were performed on a Bruker Avance DMX-500 spectrometer operating at 152.5 MHz, equipped with a 2.5-mm double-bearing MAS probe head spinning at 30 kHz. Approximately 40,000 transients were accumulated for each sample with a 0.1-s recycling delay. The chemical shifts were referenced to 1 mol L^{-1} $Ga(NO_3)_3$ solution.

2.3. Catalytic activity tests

Catalytic tests were performed in a fixed-bed flow microreactor at atmospheric pressure, with a catalyst load of 200 mg. Nitrogen was used as the carrier gas at a flow rate of 10 mL min^{-1}. The catalysts were pretreated at 773 K for 1 h in nitrogen flow, and the reaction temperature was 773 K. For dehydrogenation of propane in the absence of CO_2, the gas reactant contained 2.5 vol% propane and the balance nitrogen (N_2). For dehydrogenation of propane in the presence of carbon dioxide, the gas reactant contained 2.5 vol% propane, 5 vol% CO_2, and the balance nitrogen. The hydrocarbon reaction products were analyzed with an online gas chromatograph (Type GC-122, Shanghai) equipped with a 6-m packed column of Porapak Q and a flame ionization detector. The gas products, including N_2, CO, and CO_2, were analyzed online by another gas chromatograph equipped with a TDX-01 column and a TCD.

2.4. Transient response of the pulsed reactions

Transient response measurements of pulsed reactions were carried out at 773 K using a U-shaped quartz reactor (4 mm i.d., 400 mm long), with 100 mg of the catalyst charged into the reactor. A pulse of propylene gas was introduced through a six-port gas-sampling valve equipped with measuring tubes under a stream of CO_2 carrier gas. The signals of C_3H_6 ($M/e = 41$), CO ($M/e = 28$), and H_2 ($M/e = 2$), were recorded simultaneously by a Balzers OmniStar quadrupole mass spectrometer. Measured intensities were corrected for the relative sensitivities of the respective ions.

3. Results and discussion

3.1. Structural characterization

The powder XRD patterns of mixed Ga_2O_3–Al_2O_3 oxides with nominal Ga:Al ratios of 4:1, 1:1, and 1:4 closely resembled those of simple oxides of γ-Ga_2O_3 and γ-Al_2O_3. No diffraction lines assigned to other polymorphs of Ga_2O_3 were observed for all mixed Ga_2O_3–Al_2O_3 oxide samples, although several phases of gallium oxide (e.g., α-, β-, and δ-Ga_2O_3) are known to be present depending on the treatment conditions [32]. As shown in Fig. 1, all diffraction lines were very broad, demonstrating a low crystallinity of all of the samples. This low crystallinity is a common feature of the metastable γ-variety of both alumina and gallia polymorphs [31] and was expected due to the high surface area of the mixed Ga_2O_3–Al_2O_3 samples, for which nitrogen adsorption isotherms at 77 K gave BET surface area values ranging from 119 m^2 g^{-1} for the sample with a nominal Ga:Al ratio of 4:1 to 147 m^2 g^{-1} for Ga:Al = 1:4 (Table 1). Within this range of end values, specific surface area was found to increase monotonously with increasing aluminum content of the mixed gallia–alumina oxides.

Despite the broadness, the diffraction maxima evidenced in the XRD patterns of the gallia–alumina samples could be assigned to a single phase having the cubic spinel-type structure (space group *Fd3m*) [33], as shown by the indexing in Fig. 1. The position of the diffraction angle (2θ value) was found to decrease with increasing aluminum content of the samples, thus suggesting solid solution formation [24,31,34]. From the measured $d_{(440)}$ spacings, corresponding values of the cubic lattice parameter, a_0, were determined; these values are plotted in the inset of Fig. 1 as a function of gallium content of the mixed oxides. The a_0 values of 0.790 nm for pure γ-Al_2O_3 and 0.832 nm for pure γ-Ga_2O_3 are in good accordance with the values reported in the literature [31]. The a_0 value for the gallia–alumina mixed oxides showed an approximately linear dependence on the chemical composition. This result, taken together with the absence of any diffraction line not assignable to a single cubic phase in the corresponding XRD patterns, gives strong evidence of the formation of a series of spinel-type solid solutions with the chemical composition $Ga_xAl_{10-x}O_{15}$ ($0 < x < 10$).

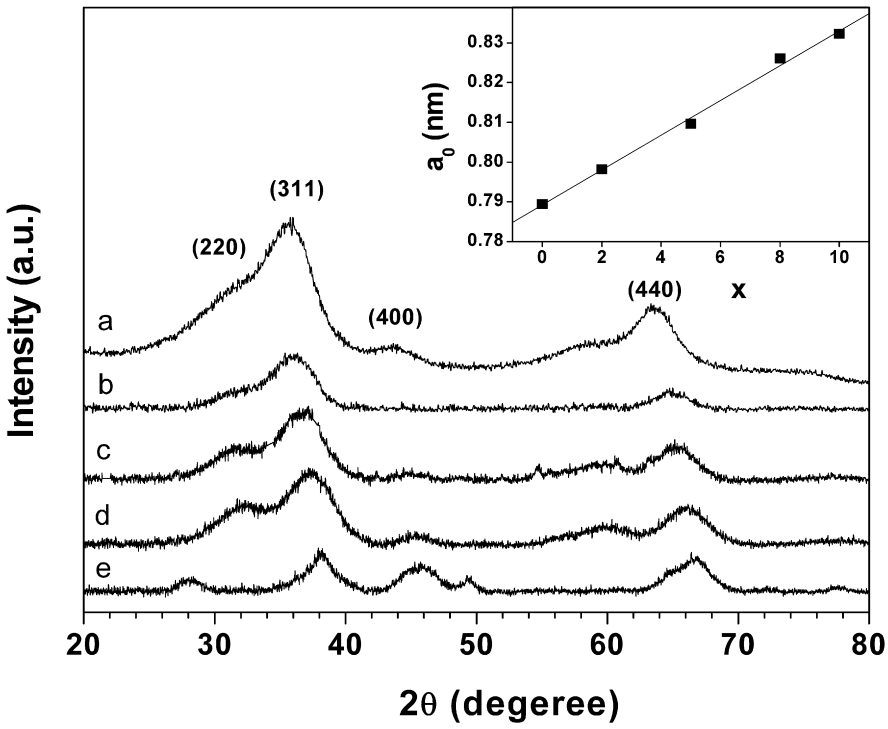

Fig. 1. XRD profiles for the $Ga_xAl_{10-x}O_{15}$ catalysts: (a) Ga_2O_3; (b) $Ga_8Al_2O_{15}$; (c) $Ga_5Al_5O_{15}$; (d) $Ga_2Al_8O_{15}$; (e) Al_2O_3. Inset: Correlation of the lattice parameter and the chemical composition for $Ga_xAl_{10-x}O_{15}$.

Table 1
Characteristics of the mixed $Ga_xAl_{10-x}O_{15}$ oxide catalysts

Sample	S_{BET}[a] ($m^2\ g^{-1}$)	Ga/Al molar ratio		$Ga_{(IV)}$[d] (%)	$Ga_{total\ (IV)}$[e] (%)	Amount of coke[f] (wt%)
		Bulk[b]	Surface[c]			
γ-Ga_2O_3	104 (58)	–	–	31	31	5.3 (4.7)
$Ga_8Al_2O_{15}$	119 (102)	4.06	3.2	41	34	4.9 (3.8)
$Ga_5Al_5O_{15}$	130 (124)	0.99	0.60	56	28	3.3 (2.1)
$Ga_2Al_8O_{15}$	147	0.26	0.18	61	13	2.9 (1.5)
γ-Al_2O_3	173	–	–	–	–	–

[a] The value outside and inside the bracket are the BET surface areas obtained before reaction and after three-round regeneration respectively.
[b] The bulk Ga/Al molar ratio calculated from the ICP data.
[c] The surface Ga/Al molar ratio based on XPS result.
[d] Percentage of Ga $_{(IV)}$ calculated from the ^{71}Ga MAS NMR results.
[e] $Ga_{IV,total}\% = \frac{n_{Ga}}{n_{Ga}+n_{Al}} \times Ga_{IV}\ \%$, $\frac{n_{Ga}}{n_{Ga}+n_{Al}}$ is the bulk molar ratio.
[f] The value outside and inside the bracket are the amount of coke deposit of the catalysts after 8 h reaction in the absence and presence of CO_2 respectively.

The ^{71}Ga MAS NMR chemical shift is known to reflect the coordination state of the Ga^{3+} ion in oxide compounds [31,34]. Fig. 2 shows the ^{71}Ga MAS NMR spectra of the mixed Ga_2O_3–Al_2O_3 samples and the γ-Ga_2O_3 sample. Two asymmetric bands, split into at least four spinning sidebands, with chemical shifts of about 180 and 10 ppm [referred to $Ga(NO_3)_3$] appeared in the NMR spectra of the $Ga_xAl_{10-x}O_{15}$ samples. According to the literature [31, 34–37], these bands are assigned to the central transition of the Ga^{3+} ion occupying tetrahedral (Ga_{IV}) and octahedral (Ga_{VI}) sites, respectively. With increasing aluminum content, a progressively increasing intensity of the line due to the tetrahedral Ga^{3+} ion (~180 ppm) was observed for the $Ga_xAl_{10-x}O_{15}$ samples, as opposed to the trend for the octahedral Ga^{3+} ion (10 ppm). A peak deconvolution of the NMR Ga_{IV} and Ga_{VI} bands provides more information about the Ga^{3+} distribution (among tetrahedral and octahedral sites) in the spinel structure. As shown in Table 1, the percentage of Ga^{3+} ions (referred to the total Ga content of the mixed oxides) found in tetrahedral sites increased markedly with decreasing Ga/Al ratio, indicating that the Ga^{3+} ions preferentially occupied the tetrahedral sites of the defect spinel structure of the γ-Ga_2O_3–Al_2O_3 solid solution [35–37]. The tetrahedral preference of Ga^{3+}, also found for many other spinels containing gallium [30, 31,38,39], can be explained in terms of a covalent contribution to the metal–oxygen bond, which is strongly developed in closed-shell d^{10} ions, such as Ga^{3+}.

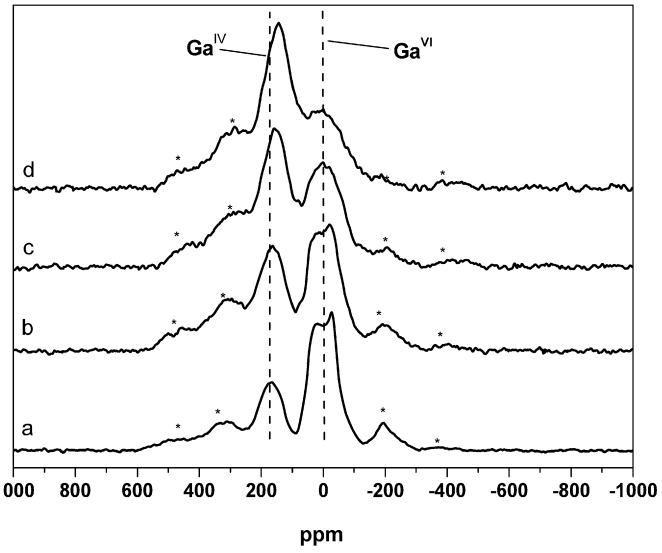

Fig. 2. ^{71}Ga MAS NMR spectra of Ga–Al catalysts: (a) Ga_2O_3; (b) $Ga_8Al_2O_{15}$; (c) $Ga_5Al_5O_{15}$; (d) $Ga_2Al_8O_{15}$. Asterisks denote spinning sidebands.

3.2. Surface acidity measurements

The surface acidity of the mixed Ga_2O_3–Al_2O_3 oxides, as well as simple oxides of γ-Ga_2O_3 and γ-Al_2O_3, was measured by the NH_3-TPD method. Because of the site's low density and moderate strength, the samples were flushed with nitrogen after ammonia

Table 2
Summary of NH_3-TPD measurements

Catalyst	Peak temperature (K)		NH_3 desorbed					
	α	β	α (393–623 K)		β (673–800 K)		Total	
			mmol g_{cat}^{-1}	μmol m_{cat}^{-2}	mmol g_{cat}^{-1}	μmol m_{cat}^{-2}	mmol g_{cat}^{-1}	μmol m_{cat}^{-2}
γ-Ga_2O_3	480	754	0.47	4.5	0.03	0.3	0.5	4.8
$Ga_8Al_2O_{15}$	479	756	0.6	5.0	0.06	0.5	0.66	5.5
$Ga_5Al_5O_{15}$	489	757	0.55	4.2	0.11	0.8	0.66	5.0
$Ga_2Al_8O_{15}$	481	758	0.53	3.4	0.14	0.9	0.67	4.4
γ-Al_2O_3	493	758	0.51	2.9	0.18	1	0.69	3.9

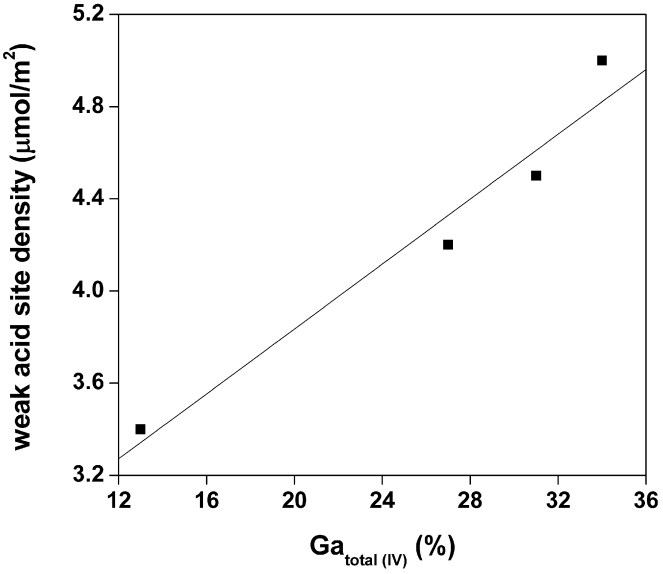

Fig. 3. Correlation of weak acid site amount and percentage of $Ga_{total\,(IV)}$.

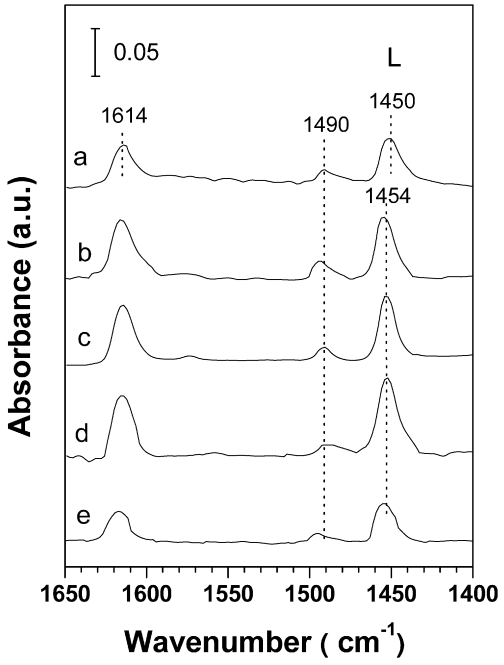

Fig. 4. IR spectra of pyridine adsorbed on $Ga_xAl_{10-x}O_{15}$ catalysts at 473 K: (a) Ga_2O_3; (b) $Ga_8Al_2O_{15}$; (c) $Ga_5Al_5O_{15}$; (d) $Ga_2Al_8O_{15}$; (e) Al_2O_3.

adsorption at a low temperature (393 K) before the TPD measurements. All of the samples exhibited two desorption peaks: a broad peak at 393–623 K and a smaller peak at 673–800 K, corresponding to acid sites of weak and medium strength, respectively [23]. The relative acid values obtained from the NH_3-TPD measurements are given in Table 2. Because no obvious relationship between the surface acidity of the oxides and the composition of the mixed oxides was observed, we correlated the specific acid site density (expressed in terms of μmol m^{-2}) and the Ga^{3+} distribution based on the ^{71}Ga NMR data. The results, given in Fig. 3, show that the weak acid site density for the gallia–alumina mixed oxides is an approximately linear function of the tetrahedral Ga^{3+} population. This result, in conjunction with much higher population of weak acid sites relative to medium sites, suggests the essential role of tetrahedral surface Ga^{3+} sites in creating the surface acidity of the mixed oxides [40,41].

Additional insight into the acid nature of the catalysts was gained from the pyridine adsorption coupled with FTIR measurements reported in Fig. 4. The results show that pyridine adsorption on fresh catalysts at room temperature, followed by evacuation at 423 K, gave rise to three characteristic IR bands at 1614 cm^{-1} (ν_{8a}), 1490 cm^{+1} (ν_{19a}), and ca. 1452 cm^{-1} (ν_{19b}), which can be assigned to pyridine species interacting with Lewis acid sites [34,40,42]. According to the literature data, these Lewis acid sites are related to coordinatively unsaturated (cus) Ga^{3+} or Al^{3+} ions in the tetrahedral position [40]. No bands were observed at 1640 or 1545 cm^{-1} in the spectra corresponding to pyridinium ions, indicating that the material under study has no Brønsted acid sites of sufficient strength to protonate the adsorbed molecule [42]. It is noteworthy that an appreciable increase in the intensity of the ν_{19b} band of adsorbed pyridine also has been identified for the mixed-oxide catalysts with respect to the simple oxide of γ-Ga_2O_3, further confirming the greater surface density of Lewis acid sites that can be achieved over the mixed-oxide materials.

3.3. Dehydrogenation of propane

The dehydrogenation of propane to propylene over the five mixed- or single-oxide catalysts in the presence or absence of CO_2 was investigated at 773 K. The major product formed in the reaction was propylene, and the minor products were ethane, ethylene, and methane. Note that the aromatization of propane occurring predominantly over Ga-ZSM-5 systems [43] was not identified in the present study, possibly due to the absence of $Ga^{\delta+}$ ($\delta < 2$) species on XPS measurements (not shown). The results, reported in Table 3, point to a marked composition effect on the catalytic performance of the $Ga_xAl_{10-x}O_{15}$ samples. The simple oxide of γ-Al_2O_3 demonstrated very low activity, consistent with the inferior activity of alumina and other metal oxides reported in the literature [20], indicating that the presence of Ga species is indispensable to the genesis of catalytically active sites for alkane dehydrogenation. For all of the Ga-containing materials, the selectivity to propylene was always high (>91%), whereas the highest conversion of propane was 51.7%. The initial conversion of propane on the catalysts decreased in the order $Ga_8Al_2O_{15} > \gamma$-$Ga_2O_3 > Ga_5Al_5O_{15} > Ga_2Al_8O_{15}$, with the same tendency observed for the specific activity normalized by BET surface area. This demonstrates that despite its lower Ga_2O_3 content, a γ-Ga_2O_3–Al_2O_3 solid solu-

Table 3
Reaction data in the presence or absence of carbon dioxide

Catalyst	In the presence of CO_2[a]			In the absence of CO_2[a]		
	$C_{propane}$[b] (%)	$S_{propylene}$[c] (%)	Activity[d] ($\mu mol\ h^{-1}\ m^{-2}$)	$C_{propane}$[b] (%)	$S_{propylene}$[c] (%)	Activity[d] ($\mu mol\ h^{-1}\ m^{-2}$)
γ-Ga_2O_3	35.9 (17.0)	97.2 (98.2)	12 (5.5)	41.3 (11.6)	93.3 (98.3)	13 (3.7)
$Ga_8Al_2O_{15}$	49.7 (33.1)	91.7 (98.0)	14 (10)	51.7 (22.5)	91.6 (98.2)	15 (6.3)
$Ga_5Al_5O_{15}$	33.7 (28.0)	92.9 (97.1)	8.5 (7.0)	38.4 (22.3)	92.3 (98.0)	10 (5.5)
$Ga_2Al_8O_{15}$	19.3 (18.0)	92.9 (95.0)	4.4 (4.2)	22.8 (21.9)	94.9 (97.2)	5.2 (5.0)
γ-Al_2O_3	2.2 (0.5)	92.5 (88.4)	0.44 (0.1)	2.8 (0.6)	91.3 (84.2)	0.56 (0.1)

[a] The value outside and inside the bracket are the data obtained at 0.25 and 8 h respectively.
[b] Conversion of propane.
[c] Selectivity to propylene.
[d] Specific activity normalized by BET surface area.

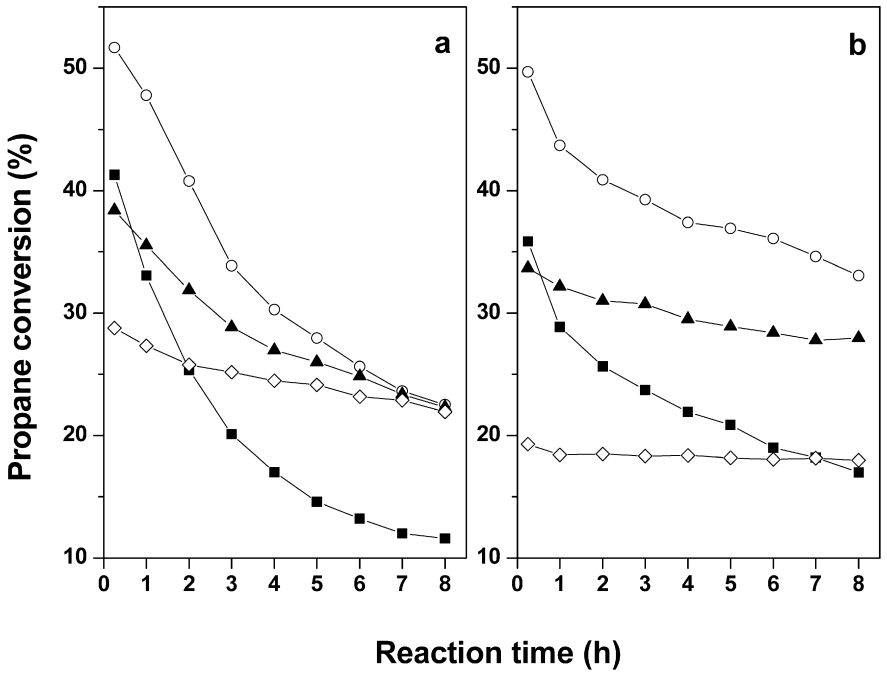

Fig. 5. Conversions of propane for $Ga_xAl_{10-x}O_{15}$ catalysts at 773 K (a) in the absence and (b) in the presence of carbon dioxide: (■) Ga_2O_3; (○) $Ga_8Al_2O_{15}$; (▲) $Ga_5Al_5O_{15}$; (◇) $Ga_2Al_8O_{15}$.

tion with suitable composition can be even more active than bulk γ-Ga_2O_3. Moreover, the promoting role of carbon dioxide in the dehydrogenation of propane was not observed in all samples. Such a negative effect was previously reported by Xu et al. over Al_2O_3- and ZrO_2-supported gallium oxide catalysts [23]. This unexpected phenomenon has been attributed to the greatly reduced propane adsorption capacity when CO_2 is introduced into these systems [21,23].

Fig. 5 characterizes the catalytic performance in both processes as a function of reaction time. For all of the catalysts, propane conversion decreased with increasing reaction time. Thus decreased propene yield can be attributed to carbon deposition on the surface of Ga_2O_3-based materials, as suggested in previous work [24,25]. With the γ-Ga_2O_3 catalyst, rapid deactivation of the catalyst in both the presence and absence of carbon dioxide was seen, and conversion of propane decreased from 35.9 to 17% and from 41.3 to 11.6% within 8 h, respectively. In contrast, the propylene yields were increased markedly by the introduction of aluminum in both the presence and absence of carbon dioxide in the runs for 8 h. In addition, propane conversion of the $Ga_xAl_{10-x}O_{15}$ catalysts at steady state were considerably higher in the presence of carbon dioxide than in the absence of carbon dioxide, indicating remarkable stability as a function of time on stream. The amounts of coke deposited on the four Ga-containing catalysts in both processes evaluated by TGA, given in Table 1, indicate that the markedly enhanced stability of the $Ga_xAl_{10-x}O_{15}$ catalysts in the presence of CO_2 may be due to their low coking tendency as a function of time on stream, which appears to be rather unique in this type of application.

Previous investigations of the use of Ga_2O_3-based catalysts for ethane or propane dehydrogenation have found that various parameters, including the nature of the support, the coordination state and reducibility of gallium species, and the acid/base properties and gallium content of the catalysts, must be considered to account for the observed catalytic behavior in the dehydrogenation of light alkanes [4,21–25]. Generally, a catalyst with a high surface acid site density performs better in the dehydrogenation of alkanes [24]. To clarify the dependence of the catalytic activity on incorporation of aluminum, Fig. 6 illustrates the correlation between the initial activity of the $Ga_xAl_{10-x}O_{15}$ catalysts in the presence of CO_2 and the density of both weak and medium-strong acid sites as determined by NH_3-TPD. Whereas the variation of surface weak acid site density demonstrated excellent correlation with the corresponding propane conversion rates, a negative correlation was identified between activity and medium-strong acid site density. This indicates that weak surface acidity (specifically, weak Lewis acid site density of the surface), not medium-strong surface acidity, is crucial to achieving high activity and stability. This result,

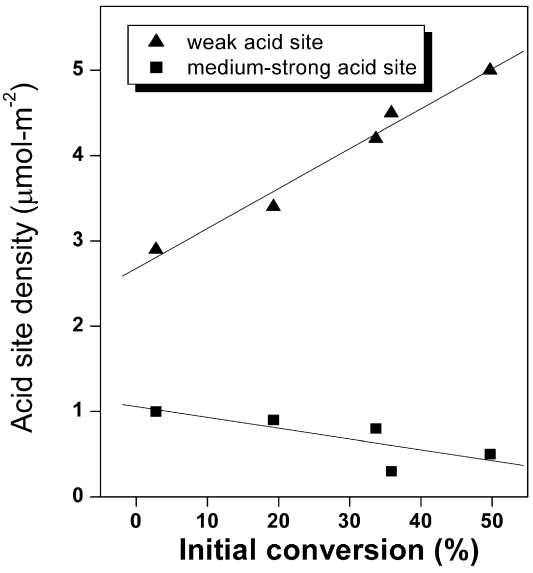

Fig. 6. Acid site amount per surface area versus conversion of propane at 0.25 h for $Ga_xAl_{10-x}O_{15}$ catalysts in the presence of carbon dioxide.

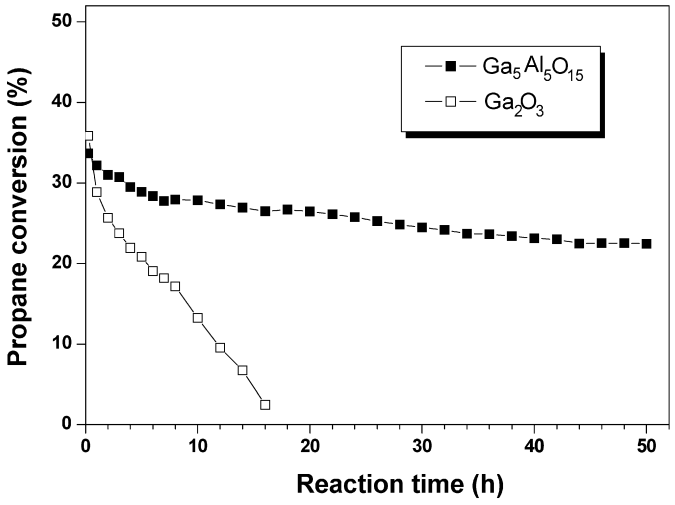

Fig. 7. Conversions of propane as a function of time on stream for $Ga_5Al_5O_{15}$ and Ga_2O_3 in the presence of carbon dioxide at 773 K.

along with the essential nature of tetrahedral Ga^{3+} population in contributing to weak surface acidity, provides strong evidence of the key role of surface tetrahedral Ga^{3+} sites in propane dehydrogenation.

The participation of surface Ga^{3+} Lewis sites in gallia-based catalysts for hydrocarbon activation has been reported [30]. In this context, it has been suggested that hydrocarbon activation proceeds on low-coordinated Ga^{3+} cations, which may play a role in the chemical activation of propane by proton abstraction, leading to the formation of propyl-gallium adspecies [23,24]. The dehydrogenation products are formed by subsequent decomposition of the resulting propyl-Ga species. A recent spectroscopic investigation by Kazansky et al. [44] found that the low-coordinated Ga^{3+} Lewis sites over gallium oxide were highly effective in the heterolytic dissociative adsorption of ethane even at room temperature. This unusual alkane activation behavior was linked to a very strong polarizability of the C–H bonds resulting from perturbation of ethane by the low-coordinated Ga^{3+} cations [44]. This may well account for the markedly improved propane dehydrogenation activity of the Ga_2O_3–Al_2O_3 solid solution materials compared with simple gallium oxide. In this respect, it appears that more active catalysts for propane dehydrogenation can be obtained by achieving a higher population of low-coordinated surface Ga^{3+} sites in the Ga_2O_3-based catalysts.

3.4. Stability and regeneration test

One of the main problems when using Ga_2O_3-based catalysts in the dehydrogenation of propane is their deactivation with time on stream [25]. To examine the likely long-term behavior of the gallia–alumina solid solution catalysts under reaction conditions, an extended 50-h on-stream operation for dehydrogenation of propane in the presence of CO_2 was carried out on the $Ga_5Al_5O_{15}$ and γ-Ga_2O_3 catalysts. As shown in Fig. 7, despite the presence of CO_2, rapid deactivation of the catalyst performance was observed for the simple oxide of γ-Ga_2O_3. After 16 h, propane conversion decreased significantly, to 2.1%. This significant decrease in propane conversion is consistent with the poor stability of Ga_2O_3-based catalysts reported in the literature [24]. Compared with the γ-Ga_2O_3 catalyst, the $Ga_5Al_5O_{15}$ sample exhibited significantly enhanced stability despite being slightly inferior to γ-Ga_2O_3 at the initial stage of the reaction. The $Ga_5Al_5O_{15}$ catalyst deactivated from an initial propane conversion value of 33.7 to 26.5% after 16 h on stream, corresponding to an activity loss of 17.2%. This loss of activity compares favorably with that of 94% for γ-Ga_2O_3 from an initial conversion of 35.9 to 2.1% after the same period of operation. It is noteworthy that even after 50 h on stream, high conversion of propane (up to 22.5%) was still maintained for $Ga_5Al_5O_{15}$. To the best of our knowledge, simple Ga_2O_3 as a dehydrogenation catalyst is inclined to deactivate rapidly, a problem that needs to be addressed [21,24]. Remarkable stability for propane dehydrogenation was recently reported for an HZSM-5-supported Ga_2O_3 catalyst at 873 K, but at the expense of marked side reactions, such as propane aromatization [25]. With high selectivity to propylene, such outstanding stability for the gallia-containing catalysts has never before been reported.

To gain more insight into the dehydrogenation of propane in the presence of CO_2 over $Ga_xAl_{10-x}O_{15}$ catalysts, a pulsed reaction technique was used to measure propylene adsorption over the catalyst [21]. Fig. 8 shows the transient response of propylene adsorption over various Ga_2O_3-based catalysts against a pulsed introduction of propylene at 773 K under a steady flow of CO_2. Nearly the same response of propylene with a similar propylene area relative to the blank runs was observed for the $Ga_2Al_8O_{15}$ catalyst; however, the propylene response was lower for the γ-Ga_2O_3, $Ga_8Al_2O_{15}$, and $Ga_5Al_5O_{15}$ catalysts than for the blank runs. In addition, the higher the gallium content, the smaller the propylene signals. It is interesting to note that although the simple oxide γ-Ga_2O_3 catalyst is characterized by a lower surface Lewis acidity, as evidenced by the NH_3-TPD and pyridine adsorption measurements, the desorption of propylene from the catalyst surface appeared to be favored on the surface of the gallia–alumina mixed oxide catalysts. Although more work is needed to clarify the unusual adsorption behavior of propylene on the weak surface Lewis acid sites, we believe that factors other than surface acidity, such as competitive adsorption due to the presence of CO_2, may play a role in determining the unique adsorption capability of the Ga–Al mixed oxide materials. Therefore, in conjunction with the coking formation data derived from TGA of the spent catalyst (Table 1), the results seem to indicate that the increased desorption of propylene from the catalyst surface is responsible for enhanced stability of the $Ga_xAl_{10-x}O_{15}$ catalysts during the catalytic dehydrogenation of propane [45–47].

Another issue of practical importance is the stability of the dehydrogenation catalyst after repeated regeneration cycles. Attempts were made to regenerate the deactivated γ-Ga_2O_3, $Ga_8Al_2O_{15}$, and $Ga_5Al_5O_{15}$ catalysts subjected to 8 h of reaction in the absence of

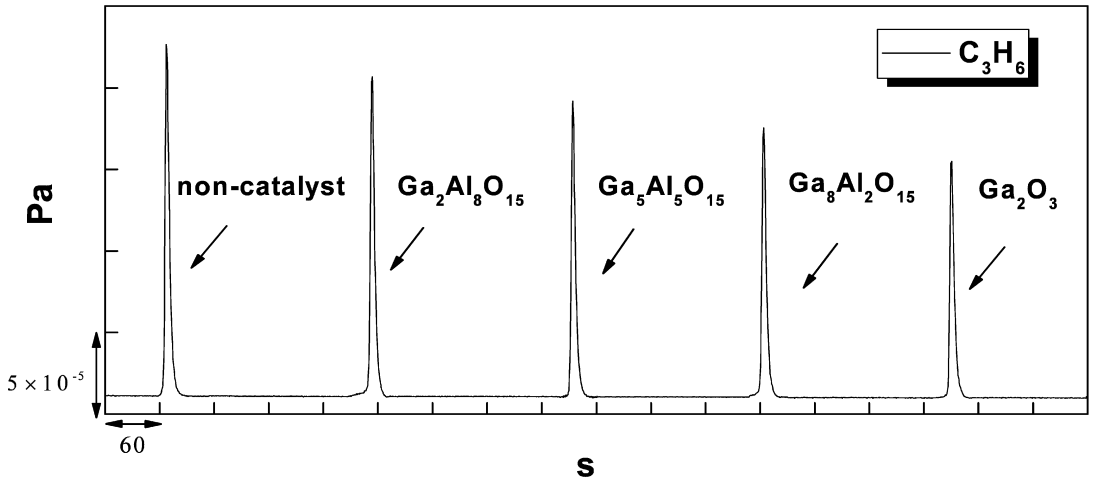

Fig. 8. Transient responses of C_3H_6 adsorption over $Ga_xAl_{10-x}O_{15}$ catalysts against a pulsed introduction of C_3H_6 under steady flow of CO_2. Reaction conditions: catalyst = 100 mg; CO_2 carrier = 25 mL min^{-1}; C_3H_6 pulse = 1 mL; furnace temperature, 773 K.

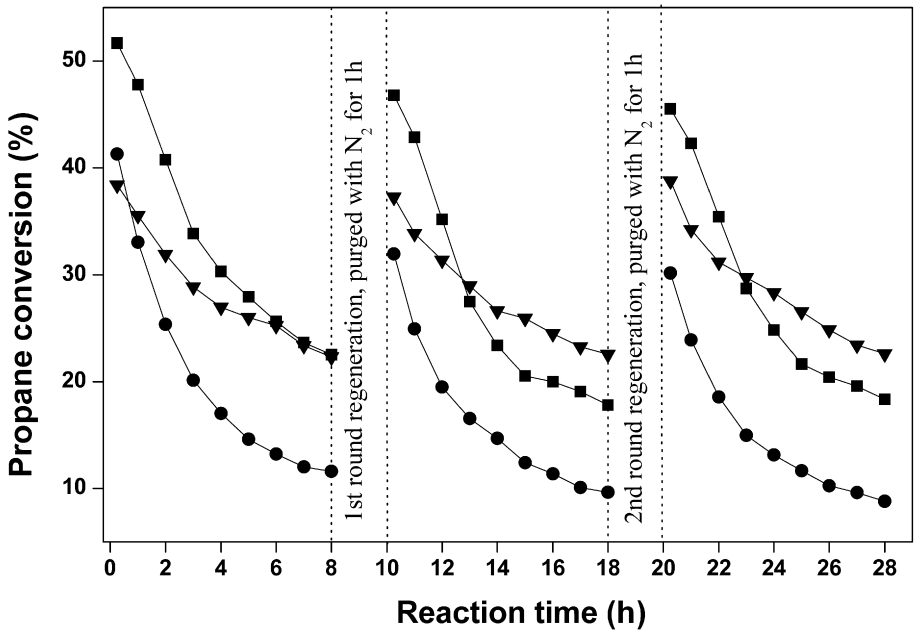

Fig. 9. Regeneration of (●) Ga_2O_3; (■) $Ga_8Al_2O_{15}$; (▼) $Ga_5Al_5O_{15}$ at 773 K.

CO_2 by recalcinating the used catalyst in flowing air at 823 K for 4 h, followed by subsequent purging with N_2. This procedure was found to be sufficient to burn off all carbon species deposited on the deactivated catalysts. As shown in Fig. 9, the $Ga_5Al_5O_{15}$ catalyst was much more stable than the other two samples. Clearly, the original activity of the $Ga_5Al_5O_{15}$ catalyst could be fully restored, with no noticeable deactivation detected even after the second regeneration. The $Ga_8Al_2O_{15}$ catalyst was deactivated from an initial conversion value of propane of 51.7% at 773 K to 45.5% after two successive reaction–regeneration cycles, corresponding to an activity loss of 11.9%. This loss of activity compares favorably with that of γ-Ga_2O_3, which exhibited poor aging properties in terms of a 26.9% loss from the initial steady conversion of 41.3 to 30.2% after completing the cycling process.

Given the thermally metastable nature of the γ-type gallium oxide materials [32,34,48], to gain further insight into the affect of repeated regeneration on the phase structure in relation to the catalytic behavior of the mixed Ga_2O_3–Al_2O_3 oxides, the phase structure of the twice-regenerated catalysts (Fig. 9) was evaluated by XRD, as shown in Fig. 10. For the γ-Ga_2O_3 sample, the major

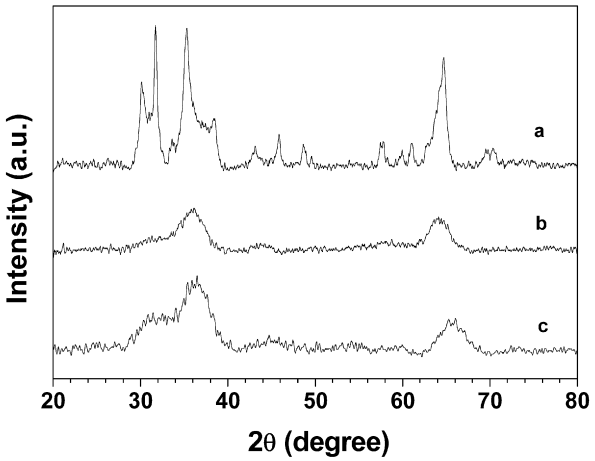

Fig. 10. Powder XRD patterns of $Ga_xAl_{10-x}O_{15}$ catalysts after three-cycle deactivation and regeneration: (a) Ga_2O_3; (b) $Ga_8Al_2O_{15}$; (c) $Ga_5Al_5O_{15}$.

phase after repeated regeneration was confirmed to be β-Ga_2O_3, which is the only stable form of Ga_2O_3 known [32,34,48]. Along with such significant phase transformation, the BET surface area of the γ-Ga_2O_3 sample also dropped dramatically to 58 $m^2\,g^{-1}$ (as shown in Table 1), which may explain the poor performance of the simple oxide of γ-Ga_2O_3 after repeated regeneration cycles. It is noteworthy that for $Ga_xAl_{10-x}O_{15}$, no significant differences were seen in the diffraction patterns obtained before (Figs. 1b, 1c) and after (Figs. 10b, 10c) the repeated regeneration, demonstrating the improved thermal stability achievable over the mixed Ga_2O_3–Al_2O_3 oxide materials. The maintenance of the γ-phase of the solid solution materials on repeated thermal treatment is further supported by the N_2 adsorption data given in Table 1. Although repeated regeneration led to a general decrease in the specific surface area, higher surface areas (>100 $m^2\,g^{-1}$) were always found for the mixed-oxide materials. Similar improved thermal stability was reported by Horiuchi et al. for alumina–gallia aerogel materials [49]. Thus, it can be concluded that the remarkable heat-tolerant nature of the Ga_2O_3–Al_2O_3 materials with favorable surface and textural properties is responsible for these materials' superior activity and stability in propane dehydrogenation.

4. Conclusion

The present work studied the catalytic dehydrogenation of propane in the presence or absence of CO_2 over a series of $Ga_xAl_{10-x}O_{15}$ mixed oxides. Among the various compositions of $Ga_xAl_{10-x}O_{15}$, the maximum initial activity and propylene yield were observed at $x = 8$. The most interesting finding of this study is the significantly enhanced stability at high conversion levels for $Ga_5Al_5O_{15}$. The enhanced catalytic activity of $Ga_xAl_{10-x}O_{15}$ mixed oxides can be linked to the abundant specific surface acid sites related to tetrahedral surface Ga^{3+} sites resulting from the formation of Ga_2O_3–Al_2O_3 solid solution in the mixed-oxide systems. Comparing the NH_3-TPD results and propane dehydrogenation activity reveals that weak surface acidity (specifically, the weak Lewis acid site density of the surface), not medium-strong surface acidity, is important for achieving high activity and stability.

Acknowledgments

This work was supported by the National Natural Science Foundation of China (20421303, 20473021, 20633030), the National High Technology Research and Development Program of China (2066AA03Z336), the National Basic Research Program of China (2003CB615807), the Shanghai Science and Technology Committee (07QH14003), and the Shanghai Education Committee (06SG03).

References

[1] M.M. Bettahar, G. Costentin, L. Savary, J.C. Lavalley, Appl. Catal. A 145 (1996) 1.
[2] M.A. Chaar, D. Patel, H.H. Kung, J. Catal. 109 (1988) 463.
[3] M.M. Bhasin, J.H. McCain, B.V. Vora, T. Imai, P.R. Pujado, Appl. Catal. A 221 (2001) 397.
[4] P. Michorczyk, J. Ogonowski, Appl. Catal. A 251 (2003) 425.
[5] M. Saito, S. Watanabe, I. Takahara, M. Inaba, K. Murata, Catal. Lett. 89 (2003) 213.
[6] Y.M. Liu, W.L. Feng, T.C. Li, H.Y. He, W.L. Dai, W. Huang, Y. Cao, K.N. Fan, J. Catal. 239 (2006) 125.
[7] Y.M. Liu, Y. Cao, N. Yi, W.L. Feng, W.L. Dai, S.R. Yan, H.Y. He, K.N. Fan, J. Catal. 224 (2004) 417.
[8] Y.M. Liu, Y. Cao, S.R. Yan, W.L. Dai, K.N. Fan, Catal. Lett. 88 (2003) 61.
[9] T. Davies, S.H. Taylor, J. Mol. Catal. A 220 (2004) 77.
[10] E. Rombi, M.G. Cutrufello, V. Solinas, S. De Rossi, G. Ferraris, A. Pistone, Appl. Catal. A 251 (2003) 255.
[11] S. Derossi, G. Ferraris, S. Fremiotti, E. Garrone, G. Ghiotti, M.C. Campa, V. Indovina, J. Catal. 148 (1994) 36.
[12] J. Gascon, C. Tellez, J. Herguido, M. Menendez, Appl. Catal. A 248 (2003) 105.
[13] Y. Zhang, Y. Zhou, A. Qiu, Y. Wang, Y. Xu, P. Wu, Catal. Commun. 7 (2006) 860.
[14] C.L. Yu, Q.J. Ge, H.Y. Xu, W.Z. Li, Ind. Eng. Chem. Res. 46 (2007) 8722.
[15] A. Virnovskaia, S. Morandi, E. Rytter, G. Ghiotti, U. Olsbye, J. Phys. Chem. C 111 (2007) 14732.
[16] S.B. Kogan, H. Schramm, M. Herskowitz, Appl. Catal. A 208 (2001) 185.
[17] H.Y. Li, Y.H. Yue, C.X. Miao, Z.K. Xie, W.M. Hua, Z. Gao, Catal. Commun. 8 (2007) 1317.
[18] P. Michorczyk, K. Gora-Marek, J. Ogonowski, Catal. Lett. 109 (2006) 195.
[19] K. Nakagawa, C. Kajita, Y. Ide, M. Okamura, S. Kato, H. Kasuya, N. Ikenaga, T. Kobayashi, T. Suzuki, Catal. Lett. 64 (2000) 215.
[20] K. Nakagawa, M. Okamura, N. Ikenaga, T. Suzuki, T. Kobayashi, Chem. Commun. (1998) 1025.
[21] K. Nakagawa, C. Kajita, K. Okumura, N.-o. Ikenaga, M. Nishitani-Gamo, T. Ando, T. Kobayashi, T. Suzuki, J. Catal. 203 (2001) 87.
[22] N.S. Nesterenko, O.A. Ponomoreva, V.V. Yuschenko, I.I. Ivanova, F. Testa, F. Di Renzo, F. Fajula, Appl. Catal. A 254 (2003) 261.
[23] B.J. Xu, B. Zheng, W.M. Hua, Y.H. Yue, Z. Gao, J. Catal. 239 (2006) 470.
[24] B. Zheng, W.M. Hua, Y.H. Yue, Z. Gao, J. Catal. 232 (2005) 143.
[25] B.J. Xu, T. Li, B. Zheng, W.M. Hua, Y.H. Yue, Z. Gao, Catal. Lett. 119 (2007) 283.
[26] M. Haneda, Y. Kintaichi, H. Hamada, Appl. Catal. B 20 (1999) 289.
[27] M. Haneda, Y. Kintaichi, H. Hamada, Appl. Catal. B 31 (2001) 251.
[28] M. Takahashi, T. Nakatani, S. Iwamoto, T. Watanabe, M. Inoue, Appl. Catal. B 70 (2007) 73.
[29] M. Haneda, Y. Kintaichi, H. Hamada, Catal. Today 54 (1999) 391.
[30] K. Shimizu, M. Takamatsu, K. Nishi, H. Yoshida, A. Satsuma, T. Tanaka, S. Yoshida, T. Hattori, J. Phys. Chem. B 103 (1999) 1542.
[31] C.O. Arean, M.R. Delgado, V. Montouillout, D. Massiot, Z. Anorg. Allg. Chem. 631 (2005) 2121.
[32] R. Roy, V.G. Hill, E.F. Osborn, J. Am. Chem. Soc. 74 (1952) 719.
[33] C.O. Arean, A.L. Bellan, M.P. Mentruit, M.R. Delgado, G.T. Palomino, Microporous Mesoporous Mater. 40 (2000) 35.
[34] J.C. Lavalley, M. Daturi, V. Montouillout, G. Clet, C.O. Arean, M.R. Delgado, A. Sahibed-dine, Phys. Chem. Chem. Phys. 5 (2003) 1301.
[35] D. Massiot, T. Vosegaard, N. Magneron, D. Trumeau, V. Montouillout, P. Berthet, T. Loiseau, B. Bujoli, Solid State NMR 15 (1999) 159.
[36] M.L. Occelli, H. Eckert, A. Wolker, A. Auroux, Microporous Mesoporous Mater. 30 (1999) 219.
[37] H.K.C. Timken, E. Oldfield, J. Am. Chem. Soc. 109 (1987) 7669.
[38] M. Takahashi, T. Nakatani, S. Iwamoto, T. Watanabe, M. Inoue, Ind. Eng. Chem. Res. 45 (2006) 3678.
[39] M. Takahashi, N. Inoue, T. Takeguchi, S. Iwamoto, M. Inoue, T. Watanabe, J. Am. Ceram. Soc. 89 (2006) 2158.
[40] A. Vimont, J.C. Lavalley, A. Sahibed-Dine, C.O. Arean, M.R. Delgado, M. Daturi, J. Phys. Chem. B 109 (2005) 9656.
[41] E.A. Gonzalez, P.V. Jasen, A. Juan, S.E. Collins, M.A. Baltanas, A.L. Bonivardi, Surf. Sci. 575 (2005) 171.
[42] M. Haneda, E. Joubert, J.C. Menezo, D. Duprez, J. Barbier, N. Bion, M. Daturi, J. Saussey, J.C. Lavalley, H. Hamada, Phys. Chem. Chem. Phys. 3 (2001) 1366.
[43] A. Montes, G. Giannetto, Appl. Catal. A 197 (2000) 31.
[44] V.B. Kazansky, I.R. Subbotina, A.A. Pronin, R. Schlogl, F.C. Jentoft, J. Phys. Chem. B 110 (2006) 7975.
[45] M.M. Bhasin, J.H. McCain, B.V. Vora, T. Imai, P.R. Pujado, Appl. Catal. A 221 (2001) 397.
[46] B. Dimon, P. Cartraud, P. Magnoux, M. Guisnet, Appl. Catal. A 101 (1993) 351.
[47] O.F. Gorriz, V. Cortes Corberan, J.L.G. Fierro, Ind. Eng. Chem. Res. 31 (1992) 2670.
[48] S.E. Collins, M.A. Baltanas, A.L. Bonivardi, J. Phys. Chem. B 110 (2006) 5498.
[49] T. Horiuchi, L.Y. Chen, T. Osaki, T. Mori, Catal. Lett. 72 (2001) 77.